Journal of Nondestructive Evaluation, Vol. 11, Nos. 3/4, 1992

Reflection of Ultrasonic Waves from Imperfect Interfaces: A Combined Boundary Element Method and Independent Scattering Model Approach

Issac Yalda-Mooshabad[1], Frank J. Margetan[1], Tim A. Gray[1], and R. Bruce Thompson[1]

Received July 10, 1992; revised August 7, 1992

A numerical technique for obtaining interface reflection coefficients for imperfect bonds between similar materials for a wide range of distributed defects is developed. A numerical boundary element method is utilized to find the far-field scattering amplitudes of a single defect for a normally incident plane wave. Then, the normal incidence reflection coefficient for a planar distribution of such defects is obtained from the independent scattering model. As a validation, the reflection coefficients are compared to the quasi-static model results where the latter are available. This establishes the basis for one application of the new model, the determination of spring constants which are not available. Other applications of the model, including studies of the response at frequencies beyond the quasi-static limit, the ratio of longitudinal to transverse wave reflectivities, and the effects of selected multiple scattering are discussed.

KEY WORDS: Ultrasonics; imperfect interfaces; quasi-static; reflection coefficients; spring constants; independent scattering; boundary element.

1. INTRODUCTION

In one category of weak solid-state bonds between similar materials, the bond plane contains a distribution of microscopic defects (e.g., cracks, voids, or contaminants). Several models, e.g., the quasi-static model (QSM) of Baik and Thompson[1] and the independent scattering model (ISM) developed by Rose,[2] have shown that reflection coefficients from these imperfect interfaces are sensitive to different characteristics of the defects. The QSM predicts bond reflectivity at low frequencies for certain defect geometries in terms of a distributed spring constant, which is defined by the deformation of the interface under static load. The reflection coefficients predicted by this model have been used to assess the detectability of imperfect bonds and to optimize bond inspections, including the selection of the angle of incidence giving maximum reflectivity.[3] However, the QSM can not be conveniently utilized for many defect distributions of interest, since the appropriate static deformation solutions are not available. An example is the prediction of the shear wave reflection from an interface containing a distribution of oblate spheroidal inclusions. Even when the static defect solutions are available, the QSM predictions are limited to the regime in which the wavelength is large with respect to the dimensional scale of the interface.

The ISM, on the other hand, computes the reflection coefficients using the scattering amplitudes for various defects at the bond-plane. Resonance information from reflectivity-vs.-frequency curves, for instance, has been used to determine the average defect size from this model.[4] In principle, the model is limited to sparse distributions of defects by its interactions between defects. In practice, it is restricted to defect geometries for

[1] Center for Nondestructive Evaluation, Iowa State University, Ames, Iowa 50011.

0195-9298/92/1200-0141$06.50/0

which scattering amplitudes are available. Moreover, it appears to lose accuracy as one approaches grazing incidence.[5]

This paper demonstrates the use of the boundary element method (BEM) to calculate the scattering amplitude required by the ISM. Since the BEM can compute the far-field scattering for an arbitrarily shaped flaw illuminated by longitudinal or transverse plane waves, its combination with the ISM produces a very powerful tool to study ultrasonic reflections from imperfect bonds for a wide variety of distributed interfacial defects. In the present work, the QSM and ISM are first reviewed. Then, the BEM is briefly described and its predictions are compared to a known exact solution. Its combination with the ISM is verified against the QSM for a specific case. Finally, several applications of this new approach are presented. These include the ability: to treat complex defect shapes, to incorporate a degree of multiple scattering, and to make reflectivity predictions at frequencies above the validity of the QSM.

2. THE QUASI-STATIC AND THE INDEPENDENT SCATTERING MODELS

2.1. The Quasi-Static Model (QSM)

Figure 1a illustrates the scattering of normally incident ultrasound from an interface between two half-spaces which is assumed to exist in the vicinity of the $x_3 = 0$ plane. In the QSM, the imperfect interface is represented by a distributed spring and mass system as shown in Fig. 1b. For a perfect interface, the boundary conditions are continuity of displacement and stress. In the QSM, the boundary conditions are modified to account for compliance and inertia changes associated with the imperfect interface.[1]

$$[\sigma(0^+) + \sigma(0^-)]/2 = \kappa[u(0^+) - u(0^-)] \quad (1)$$

$$-m\omega^2[u(0^+) + u(0^-)]/2 = \sigma(0^+) - \sigma(0^-) \quad (2)$$

where σ, κ, u, and m are the stress, the distributed spring constant per unit area, the material displacement, and the interface mass per unit area, respectively, and the coordinates 0^+ and 0^- denote the two sides of the interface. The limit that $m \to 0$ and $\kappa \to \infty$ recovers the response of a perfect interface.

The QSM uses the modified boundary conditions to predict the displacement-field reflection coefficient, R, when the ultrasonic wavelength is long compared to the interface thickness and/or lateral structure. For normally incident waves, the result, for an assumed time dependence of the form $e^{-j\omega t}$, is:

$$R_{L,T} = \frac{-j\omega(Z_{L,T}/2\kappa k_{L,t} - m/2Z_{L,T})}{(1 - m\omega^2/4\kappa_{L,T}) - j\omega(Z_{L,T}/2\kappa_{L,T} + m/2Z_{L,T})} \quad (3)$$

where the acoustic impedance $Z_{L,T}$ equals $\rho c_{L,T}$ with ρ being the density and c being the ultrasonic wave speed of the host, and where subscripts L and T indicate longitudinal and transverse waves, respectively. Note that this model implicitly includes defect interactions, which contribute to the static elasticity solution which determines κ. Note also that we have changed from the $e^{j\omega t}$ time dependence originally used by the authors[1] to coincide with the $e^{-j\omega t}$ usually used in the discussion of the boundary element method.

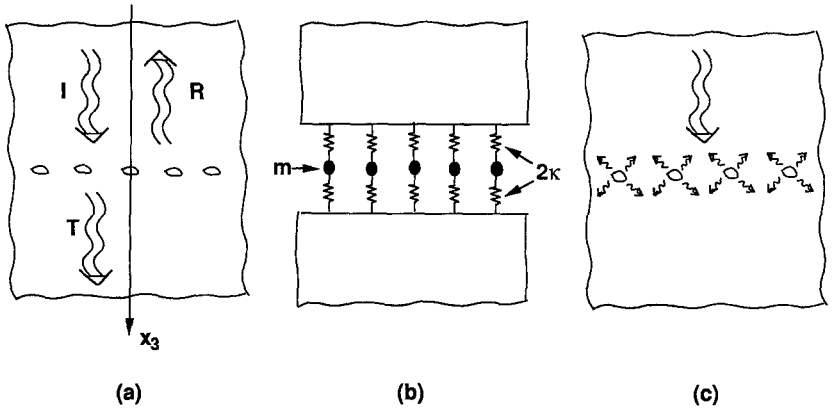

Fig. 1. Ultrasonic models for an imperfect interface: (a) geometry of ultrasonic reflection and transmission, (b) quasi-static spring model, and (c) independent scattering model.

2.2. The Independent Scattering Model (ISM)

The independent scattering model of Fig. 1c predicts the frequency dependence of the reflection coefficient for normally incident waves in terms of the scattering amplitude of single defects, with the defects assumed sufficiently far apart that their interactions can be neglected.[2] The result for normal incidence is

$$R_{L,T}(k_{L,T}) = \frac{-2\pi j}{k_{L,T}} N\bar{A}_{L,T}(k_{L,T}) \tag{4}$$

where N is the average number of defects per unit area, $\bar{A}$ is the average backscattering amplitude of one defect, and k is the wave number. This single-scattering model is expected to perform best when the area fraction of the defects is small. Note that this model, in its simplest form, does not allow for multiple scattering as shown. However, it can be extended to incorporate flaw-flaw interactions by including additional terms on the right hand side of Eq. (4) which represent selected multiple scattering effects.[4]

2.3. QSM and ISM Comparison to Experimental Measurements

To illustrate the behavior of the two models, the special case of an interface containing a distribution of identical ellipsoidal inclusions will be considered, as shown in Fig. 2. In the QSM, the interface is characterized by both a distributed mass parameter, m, and a distributed longitudinal stiffness, κ_L, whose values are given by the expressions[1]:

$$m = \frac{4\pi}{3} a_1 a_2 a_3 N(\rho_I - \rho_O) \tag{5}$$

$$\kappa_L = \frac{3(1-\nu)}{4\pi a_1^2 a_3 N}\left[2\nu\frac{e_{11}^T}{\sigma_{33}^P} + (1-\nu)\frac{e_{33}^T}{\sigma_{33}^P}\right]^{-1} \tag{6}$$

where ν, ρ_I, ρ_O, and N are the Poisson's ratio, the density of the inclusion material, the density of the host material, and the number of the defects per unit area, respectively. The a_i are the semiaxes of the inclusions in the coordinate system of Fig. 2, σ_{33}^P is the applied static stress, and e_{33}^T are the equivalent inclusion strains which can be evaluated using formulae in Ref. 1. In the derivation of Eq. (6), the inclusions have been considered to be noninteracting.

In one experimental embodiment, a thermoplastic specimen was fabricated which contained a near planar distribution of spherical nickel inclusions. The wave speeds and densities of these materials are given in Table I. The mean diameter of nickel particles was measured to be

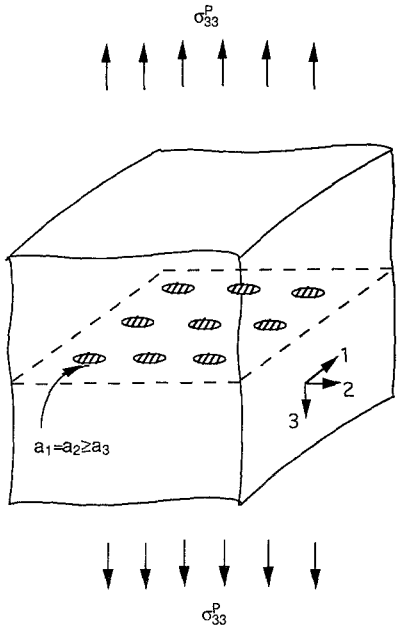

Fig. 2. Geometry of an interface containing an array of ellipsoidal inclusions in an unbounded matrix.

Table I. Material Properties Used in Calculations

Material	c_L (cm/μs)	c_T (cm/μs)	ρ (gm/cm³)
Typical	0.600	0.300	8.00
Nickel	0.604	0.300	8.90
Thermoplastic	0.266	0.134	1.18
Ti-64	0.621	0.321	4.49
Salt	0.445	0.256	2.17

79 microns, and the area fraction of the defects was calculated to be 13%. The reflection coefficients for this uniform specimen were measured[4] and are displayed in Fig. 3. The predictions of the QSM from the above formulation and of the ISM incorporating the known exact solution for backscattering from spheres are also shown in Fig. 3. Both models are in good agreement with the measurements at low frequencies, and the ISM predicts the resonance peak as well.

2.4. Conditions for Consistency of QSM and ISM

In the regime where the QSM and ISM simultaneously apply, i.e., at low frequencies and low defect area fractions, the QSM spring constant can be deduced from knowledge of the average defect scattering ampli-

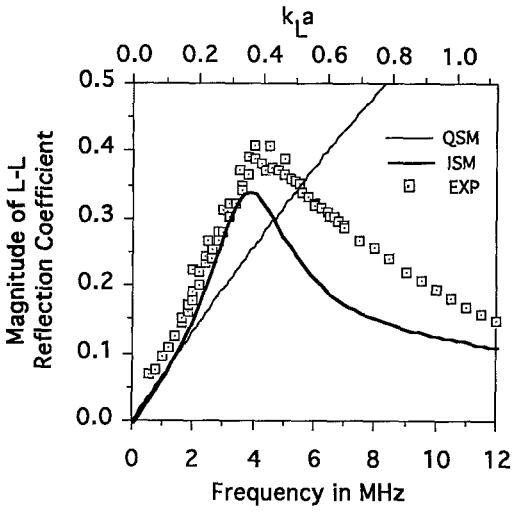

Fig. 3. Normally incident longitudinal reflection coefficients from an interface containing a planar distribution of spherical nickel particles in a thermoplastic specimen; a_1 = 40 μm and area fraction = 0.13.

tude. This deduction process can be carried out in the general case when the mass parameter of the defect distribution is non-zero. However, the mathematics is considerably simplified when $m=0$. In the following, we explicitly demonstrate the deduction procedure for a case in which the mass parameter is negligible.

At low frequencies and negligible mass, the normal-incidence reflection coefficients predicted by the QSM are reduced to the following expression:

$$R_{L,T} = \frac{-j\omega Z_{L,T}}{2\kappa_{L,T}} \tag{7}$$

Now, in the low frequency region, the average backscattering amplitude is proportional to the square of the wave number multiplied by a constant $a_{L,T}$ which can be calculated from the shape, size, and the elastic properties of the scatterer[6]:

$$\bar{A}_{L,T} = k_{L,T}^2 a_{L,T} \tag{8}$$

Then, the reflection coefficients from the ISM are given by:

$$R_{L,T} = -2\pi j N k_{L,T} a_{L,T} \tag{9}$$

Therefore, the QSM and the ISM are consistent at low frequencies if,

$$\kappa_{L,T} = \frac{\rho c_{L,T}^2}{4\pi N a_{L,T}} \tag{10}$$

Note that the interfacial stiffnesses are inversely proportional to $a_{L,T}$. Equation (10) provides a way to infer the spring constant, κ, from the ISM solution. One motivation for such an approach is the treatment of oblique incidence problems, which requires knowledge of both the κ_L and κ_T for QSM calculations.[3]

One can proceed in a similar manner if m is non-negligible, although the final expression for $\kappa_{L,T}$ is more complicated. We note that there is no difficulty in calculating the QSM mass parameter when the defect morphology is known. m is essentially the total volume of the defects multiplied by the density difference between the defect and the host material.

3. COMBINATION OF BOUNDARY ELEMENT METHOD AND ISM

3.1. The Boundary Element Method (BEM)

The field scattered from a single inhomogeneity, $\vec{u}^{sc}$, is characterized by a scattering amplitude, A, which defines the spherically spreading wave that is generated in the far-field by the plane wave illumination of the flaw as shown in Fig. 4. For elastic waves:

$$\frac{\vec{u}^{sc}\hat{d}^{sc}}{|\vec{u}^{in}|} \rightarrow \frac{A(\theta^{in},\phi^{in},\hat{d}^{in},\theta^{sc},\phi^{sc},\hat{d}^{sc})}{r} e^{jk_{L,T}r} \tag{11}$$

with r large, where A is a function of the incident and scattered directions (θ,ϕ), polarizations $(\hat{d})$, and wave

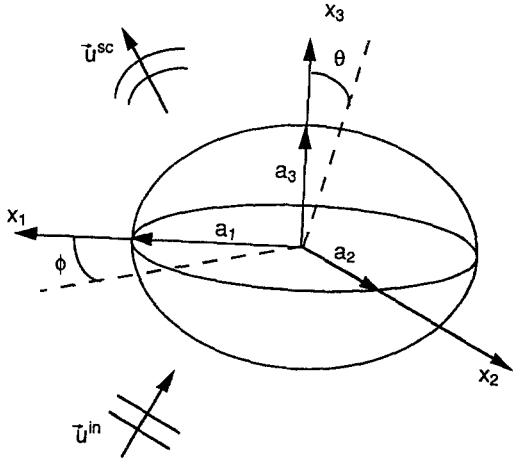

Fig. 4. General scattering problem.

numbers, r is the distance from the apparent source of the spherical wave, $|\vec{u}^{in}|$ is the amplitude of the incident plane wave.[7]

The numerical BEM for calculating the scattering amplitude begins with the generation of a mesh of surface area elements which cover the flaw. The shape of the flaw can in principle be arbitrary. Each area element has node points at selected locations on its perimeter. The BEM for solving elastodynamics scattering problem makes use of a boundary integral equation (BIE). The BIE is written for the host medium and the flaw material at the same node points. Interface displacements and tractions are matched-up resulting in a set of simultaneous, linear algebraic equations which are then solved by matrix inversion techniques.[7]

To illustrate the BEM, we have used it to calculate the scattering amplitude for L-wave backscatter from a 30-μm radius spherical void in a "typical" host metal (see Table I). The BEM results at selected frequencies are compared to known exact solutions[8] in Fig. 5. The BEM predictions using a 40-elements mesh and a 140-elements mesh are found to be in good agreement with the exact solution at low frequencies. As the frequency increases, the 140-elements model does a better job than the 40-elements model. In general, finer meshes are required as the frequency increases since the surface solution has a correspondingly shorter length scale.[7]

3.2. Comparison of BEM+ISM and QSM Predictions at Long Wavelength

We now demonstrate how the BEM and ISM may be combined to predict reflection coefficients for defect distributions. We consider a planar distribution of spheroidal cavities ($a_1 = a_2 \leq a_3$) in a "typical" metal. The cavities have a fixed in-plane dimension (a_1) and number density, and are illuminated by longitudinal waves at a fixed frequency ($k_L a = \pi/20$). The fraction of the interfacial plane covered by the cavities is 0.025. The BEM was used to calculate single-cavity L-wave scattering amplitude for different aspect ratios (ratio of out-of-plane and in-plane dimensions), and the ISM was subsequently used to calculate the corresponding interface reflection coefficients. The BEM+ISM predictions are compared to those of the QSM, as a function of aspect ratio, in Fig. 6. For this low-frequency calculation, the two models match up very well for moderate aspect ratios. But as the aspect ratio decreases below 0.05, i.e., the spheroids become very thin, the numerical BEM breaks down. This is due to the singular nature of the surface integration when the opposing faces of the spheroid are in close proximity.[9] Krishnasamy *et al.*[10] have presented a combined conventional and hypersingular boundary integral formulation for scattering of waves from slender voids which is free of these problems.

4. APPLICATIONS OF BEM+ISM

4.1. Determination of Spring Constants for the QSM

An attractive property of the QSM is its ability to predict interface transmission and reflection coefficients at arbitrary angles of incidence, given the mass parameter and spring constants.[3] However, use of that model is restricted by the fact that the relationship of the spring

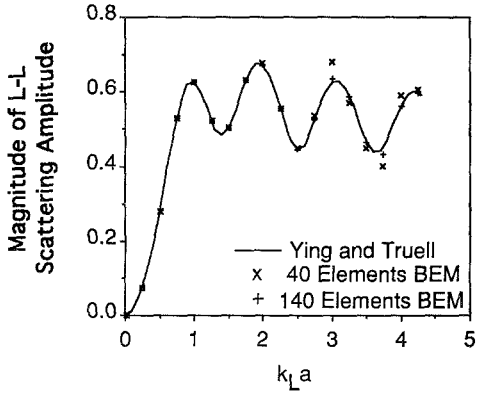

Fig. 5. Far-field backscattering amplitude of a spherical void illuminated by a normally incident longitudinal wave, a_1 = 30 μm.

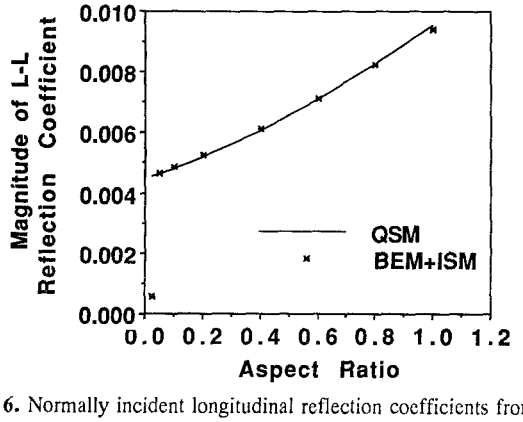

Fig. 6. Normally incident longitudinal reflection coefficients from an interface containing a distribution of spheroidal voids; $k_L a_1 = \pi/20$ and area fraction = 0.025.

constant to the defect morphology is limited to a few geometries for which appropriate static elasticity solutions are readily available. This range of cases can be greatly extended through use of Eq. (10), where $a_{L,T}$ is evaluated from the BEM.

Considering the spheroidal void case of the previous example, a simple expression (i.e., Eq. (6) is available for the longitudinal wave spring constant, κ_L, but not for the transverse wave constant, κ_T. The longitudinal spring constants for distributions of such voids, as predicted by the QSM and the BEM + ISM, are listed in Table II for several choices of the aspect ratio. This data, which is essentially the same as that plotted in Fig. 6, establishes in greater detail the accuracy of the BEM + ISM approach. Moreover, the combined BEM + ISM model predicts the transverse wave spring constants (also listed in Table II) which are not otherwise known to the authors. It is interesting to note that the shear stiffness is much more strongly influenced by the aspect ratio of the voids than the longitudinal stiffness. The BEM can readily treat voids and inclusions of more complex shape as well.

4.2. Response at Higher Frequencies

The QSM is restricted to lower frequencies, where the wavelength is large with respect to the size and separation of the elementary defects. The combined BEM + ISM, on the other hand, can be used to predict reflection coefficients at higher frequencies. Figure 3 presented the related example of the scattering from a distribution of spherical inclusions. This demonstrated the ability of the ISM to predict high-frequency response where the QSM failed. In that case, however, the BEM was not needed, since a solution for scattering amplitude based on separation of variables was available. In studies of the scattering of ultrasound from bond lines in diffusion-bonded titanium alloys, similar reflectivity predictions are often desired for inclusions of more complex shape for which the scattering amplitude is not readily available. For example, in one recent study,[4] an aircraft engine manufacturer identified four substances as possible bond-plane contaminants in the factory environment. Diffusion bonded titanium specimens incorporating each of these contaminants (feldspar, human sweat, iron rust, scouring pad particles) were manufactured for bond-plane reflectivity testing. As an example of an associated model calculation, we specifically consider the case of contamination by human sweat deposits. In a first approximation, the embedded contaminants can be modeled as thin salt particles distributed across the bond plane. For the purpose of illustration, we assume a distribution of oblate spheroidal (aspect ratio of 0.1) salt inclusions covering 10% of a bond plane in a Ti–6%Al–4%V alloy. The wave speeds and densities of Ti-64 and salt are given in Table I. Figure 7 presents the frequency dependence of the bond-plane reflection coefficients for normally incident longitudinal and transverse sound waves. Predictions are made for both the BEM + ISM and the QSM treatments. For the QSM longitudinal wave case, κ_L was determined independently using Eq. (6) to be 5095 gm/(cm·μs)². In Fig. 7a, the two models are seen to be in agreement at low frequencies as expected if the $m \neq 0$ counterpart of Eq. (10) is to hold. The two models diverge at higher frequencies illustrating the advantage of the BEM + ISM in this regime. The shear wave solution is particularly interesting since the quasi-static solution for shear interfacial stiffness is not known in this case. From the low-frequency region, a fit of the QSM to the BEM + ISM implies that the transverse interfacial stiffness constant is $\kappa_T = 2067$ gm/(cm·μs)². Based on this value, the QSM shear-wave reflection coefficient at higher frequencies has been predicted as shown in Fig. 7b.

Table II. Spring Constants for a Sparse Distribution of Spheroidal Voids in "Typical" Material from the QSM and BEM + ISM[a]

Aspect ratio a_3/a_1	(κ_L)QSM (gm/[cm.μs]²)	(κ_L)BEM + ISM (gm/[cm.μs]²)	(κ_T)BEM + ISM (gm/[cm.μs]²)
0.05	16,835	16,660	12,680
0.10	16,670	16,350	11,526
0.20	16,236	15,930	9,725
0.40	15,048	14,834	7,294
0.60	13,652	13,555	5,776
0.80	12,255	12,269	4,766
1.00	10,946	11,081	4,063

[a]The area fraction was taken to be 2.5% in all cases.

4.3. Ratio of Longitudinal to Transverse Wave Reflectivities

For a distribution of microscopic defects, Nagy and Adler[6] have defined characteristic frequencies, Ω, at which the magnitude of the reflection and transmission coefficients are equal. When the QSM applies and the mass parameter is negligible, the ratio of transverse to longitudinal characteristic frequencies is found to be:

$$\frac{\Omega_T}{\Omega_L} = \frac{\kappa_T c_L}{\kappa_L c_T} = \lim_{\omega \to 0} \frac{R_L}{R_T} \tag{12}$$

when $m \neq 0$, the ratio of characteristic frequencies is a

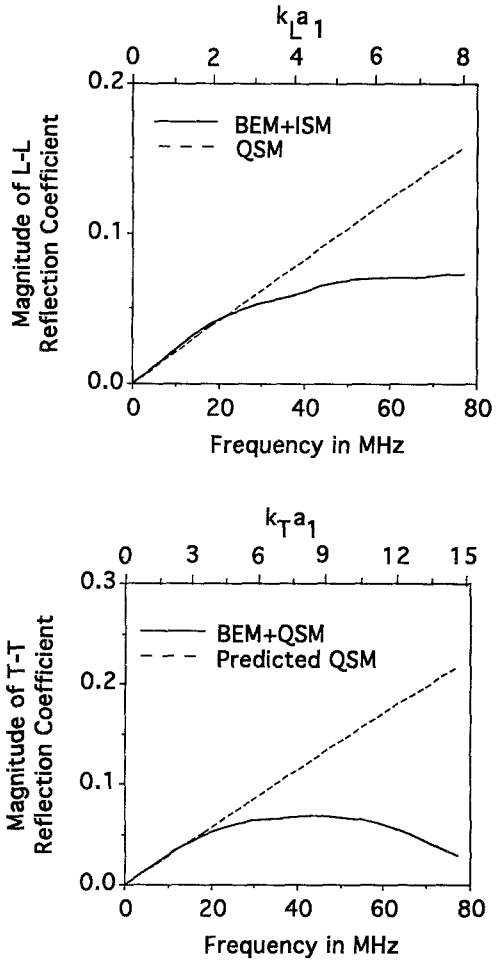

Fig. 7. Normally incident longitudinal reflection coefficients from an interface containing a distribution of spheroidal salt particles in a Ti-64 specimen; a_1 = 100 μm, aspect ratio = 0.1, and area fraction = 0.1: (a) longitudinal, and (b) transverse.

more complicated function of m, κ_L, κ_T. In the QSM model, the reflection coefficient rises and approaches unity as the frequency increases. There is consequently no difficulty in locating the characteristic frequency at which the reflection and transmission coefficients are equal. In practice, however, the reflection coefficient initially rises with frequency, but may then undergo undulating behavior associated with resonances in the single defect scattering amplitude. There may be no frequency for which reflection and transmission coefficients are equal. This is demonstrated in Fig. 3 for example. It has been suggested that this ratio is closely related to the physical nature of the interface imperfections.[6] Nagy and Adler observed experimentally that this ratio was greater than 1.4 for diffusion bonds (ranging from 1.5 to 2 in titanium) and less than 1.4 for compressed surfaces (ranging from 0.6 to 0.9 in measurements in aluminum and steel). The later were taken as models of "kissing bonds," in which the mating surfaces are in close contact but in which little mechanical bonding had occurred.

Motivated by a preliminary calculation of the effect of aspect ratio on $\text{limit}_{\omega \to 0} R_L/R_T$, as reported by Nagy and Adler based on evaluation of κ_L from static elasticity solutions,[6] we have computed the same ratio using the BEM + ISM formalism. We assumed spheroidal voids in Ti-64 having a fixed in-plane dimension ($a_1 = a_2 = 100$ μm) and a fixed area fraction (0.1). For each assumed aspect ratio (a_3/a_1) and incident wave type, the BEM was used to determine the single-void scattering amplitudes at frequencies in the range 1 MHz$\leq\omega\leq$10 MHz. The ISM was then used to determine the reflection coefficients at these frequencies, and the ratio of R_L/R_T was calculated. This ratio was found to rapidly converge as ω decreased. The results, shown in Fig. 8, range from 1.4 at an aspect ratio of 0.05 (crack-like defects) to 0.6 at unity aspect ratio (spheres). They differ somewhat from the previous calculation[6] in that our results show a greater range in the reflection coefficient ratio. Our predictions are in good agreement with the experimental observations if one assumes that the microdefects in compressive or "kissing" bonds have high aspect ratios, consistent with the original hypothesis of Nagy and Adler.

4.4. Multiple Scattering Effects

The ISM, as stated by Eq. (4), neglects multiple scattering effects. However, Rose has provided a for-

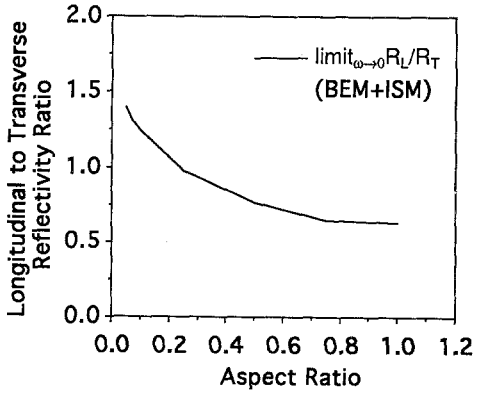

Fig. 8. Ratio of longitudinal to transverse reflection coefficients from an interface containing a distribution of spheroidal voids in a Ti-64 specimen; a_1 = 100 μm and area fraction = 0.1.

malism[2] and Margetan *et al.* have provided a specific example[4] for inclusion of nearest neighbor interactions. Consider here the case in which the defects are arranged in square arrays. The second order effect associated with scattering from one inhomogeneity to its nearest neighbors is shown in the diagram of Fig. 9a. The total average backscatter amplitude from the central defect for normally incident waves, including the second order contributions from its nearest neighbors, $\bar{B}$, is approximately given by:

$$\begin{aligned}\bar{B}_{L-L}(0^{in},180^{sc}) &= \bar{A}_{L-L}(0^{in},180^{sc}) \\ &+ n_1\left[\bar{A}_{L-L}(0^{in},90^{sc})\bar{A}_{L-L}(90^{in},180^{sc})\frac{e^{jk_L d_1}}{d_1}\right. \\ &\left. + \bar{A}_{L-T}(0^{in},90^{sc})\bar{A}_{T-L}(90^{in},180^{sc})\frac{e^{jk_T d_1}}{d_1}\right] \\ &+ n_2\left[\bar{A}_{L-L}(0^{in},90^{sc})\bar{A}_{L-L}(90^{in},180^{sc})\frac{e^{jk_L d_2}}{d_2}\right. \\ &\left. + \bar{A}_{L-T}(0^{in},90^{sc})\bar{A}_{T-L}(90^{in},180^{sc})\frac{e^{jk_T d_2}}{d_2}\right]\end{aligned} \quad (13)$$

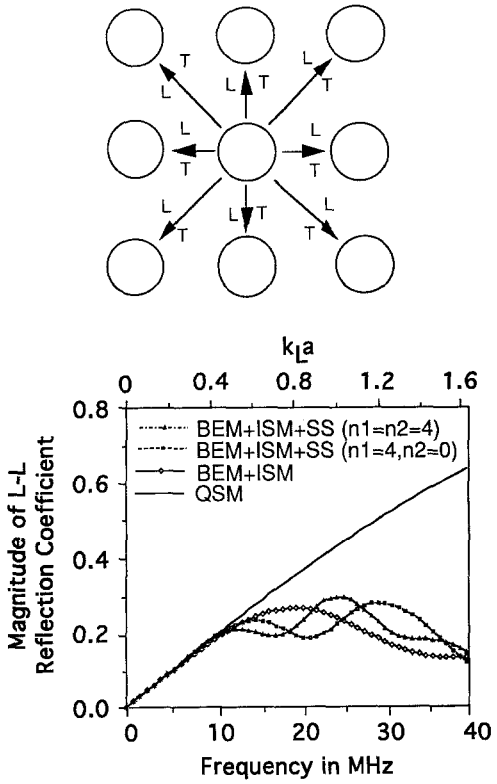

Fig. 9. An interface containing a distribution of spherical voids in a Ti-64 diffusion-bonded specimen and illuminated by a normally incident longitudinal wave: (a) propagation of second order effects from one scatterer to its nearest neighbors in the bond plane, and (b) reflection coefficients, a_1 = 40 μm and area fraction = 0.2.

where n_1 and n_2 are the numbers of the nearest and next-nearest neighbors of the central defect, respectively, and d_1 and d_2 are the corresponding separations. The secondary backscattering includes the *L-L-L* and *L-T-L* soundpaths. This analytical formulation is based on the far-field approximation, which represents the wave scattered from one flaw to the other in its far-field form. At low frequencies, this approximation does not fully capture interactions because the use of far-field scattering amplitudes is not appropriate when defect separation is on the order of a wavelength. The accuracy of this approach, for the case of treating the scattering from two defects, has been examined in detail by Schafbuch *et al.*[11] The ISM is extended to include secondary scattering (SS) effect by replacing $\bar{A}$ in Eq. (4) $\bar{B}$ from Eq. (13). The normally incident longitudinal wave reflection coefficients for a distribution of spherical voids with 20% area fraction in a Ti-64 specimen have been calculated for four models and are shown in Fig. 9b. The first two models are the QSM and the combined BEM + ISM neglecting multiple scattering. The other two model treatments include secondary scattering contributions from the interactions with first and the first and second set of nearest neighbors, respectively. These multiple scattering models show secondary resonance peaks due to defect interactions.

5. CONCLUSIONS

The BEM may be used to predict scattering from defects of arbitrary shapes (voids or inclusions) for intermediate frequency ranges with a general incident field. The ISM relates the scattering from a single defect to that of a distribution of defects when the interactions can be neglected. The BEM + ISM has been shown to be an effective tool in predicting the scattering from imperfectly joined interfaces. The predicted bond reflectivities from the combined BEM + ISM match well with the QSM predictions at long wavelengths where the QSM is valid. The combined BEM + ISM method is able to directly predict reflectivities for wide varieties of defect distributions, and can be used to obtain the transverse and longitudinal interfacial stiffnesses required as inputs for the QSM. The combined model allows extension to frequencies when the wavelength is on the order of defect dimensions, and has been used to show that the longitudinal to transverse wave reflectivities ratio of an imperfect interface depends on the shape of the scattering defects. The BEM + ISM model can be extended to include multiple scattering effects, but this extension does not capture all interactions at long wavelengths because

of the breakdown of the far-field approximation employed. In such cases, a full BEM approach is required.

ACKNOWLEDGMENTS

This work was supported by Pratt & Whitney Aircraft under P. O. #F452635, which was a subcontract to a program sponsored by the Air Force Wright Aeronautical Laboratories/Materials Laboratory. The work was performed at the Center for Nondestructive Evaluation at Iowa State University. The authors wish to thank Paul J. Schafbuch for the use of his boundary element code of solitary elastic wave scatterers.

REFERENCES

1. J.-M. Baik and R. B. Thompson, Ultrasonic scattering from imperfect interfaces: A quasi-static model, *J. Nondestr. Eval.* **4**:177–196 (1984).
2. J. H. Rose, Ultrasonic reflectivity of diffusion bonds, in *Review of Progress in Quantitative Nondestructive Evaluation*, D. O. Thompson and D. E. Chimenti, eds. (Plenum Press, New York, 1989), Vol. 8B, pp. 1925–1931.
3. F. J. Margetan, R. B. Thompson, and T. A. Gray, Interfacial spring model for ultrasonic interactions with imperfect interfaces: Theory of oblique incidence and application to diffusion bonded butt joints, *J. Nondestr. Eval.* **7**:131–152 (1988).
4. F. J. Margetan, R. B. Thompson, T. A. Gray, and J. H. Rose, Experimental studies pertaining to the interaction of ultrasound with metal–metal bonds, in *Review of Progress in Quantitative Nondestructive Evaluation*, D. O. Thompson and D. E. Chimenti, eds. (Plenum Press, New York, 1990), Vol. 9B, pp. 1323–1330.
5. J. H. Rose, private communication.
6. P. B. Nagy and L. Adler, Reflection of ultrasonic waves at imperfect boundaries, in *Review of Progress in Quantitative Nondestructive Evaluation*, D. O. Thompson and D. E. Chimenti, eds. (Plenum Press, New York, 1991), Vol. 10A, pp. 177–184.
7. P. J. Schafbuch, R. B. Thompson, and F. J. Rizzo, Application of boundary element method to elastic wave scattering by irregular defects, *J. Nondestr. Eval.* **9**:113–127 (1991).
8. C. F. Ying and R. Truell, Scattering of a plane longitudinal wave by a spherical obstacle in an isotropically elastic solid, *J. Appl. Phys.* **27**:1086–1097 (1956).
9. P. J. Schafbuch, F. J. Rizzo, and R. B. Thompson, Boundary element method solutions for elastic wave scattering in 3D, *Int. J. Num. Meth. Engr.* (in press).
10. G. Krishnasamy, F. J. Rizzo, and Y. Liu, Scattering of acoustic and elastic waves by cracklike objects: The role of hypersingular integrals, in *Review of Progress in Quantitative Nondestructive Evaluation* D. O. Thompson and D. E. Chimenti, eds. (Plenum Press, New York, 1992), Vol. 11A, pp. 25–32.
11. P. J. Schafbuch, F. J. Rizzo, and R. B. Thompson, Elastic wave scattering by multiple inclusions, in *Enhancing Analysis Techniques for Composite Materials*, L. Schwer, J. N. Reddy, and A. Mal, eds. (ASME Publication NDE-Vol. 10, ASME, New York, 1991), pp. 103–111.